Davis, J.M., et al., 2021, A record of syn-tectonic sedimentation revealed by perched alluvial fan deposits in Valles Marineris, Mars: Geology, v. 49, https://doi.org/10.1130/G48971.1

A Record of Syn-Tectonic Sedimentation Revealed by Perched Alluvial Fan Deposits in Valles Marineris, Mars

Supporting Information

Joel M. Davis [1*], Peter M. Grindrod[1], Steven G. Banham[2], Nicholas H. Warner[3], Susan J. Conway[4], Sarah J. Boazman[1], and Sanjeev Gupta[3]

[1]Department of Earth Sciences, Natural History Museum, London, SW7 5HD, UK

[2]Department of Earth Science and Engineering, Imperial College, London, SW7 2BU, UK

[3]Department of Geological Sciences, State University of New York at Geneseo, Geneseo, NY, 14454, USA

[4]CNRS, UMR 6112 Laboratoire de Planétologie et Géodynamique, Université de Nantes, 44322 Nantes, France

*Corresponding author: joel.davis@nhm.ac.uk

This file contains the detailed methods relating to the production of the stereo CTX mosaic as well as the morphometrics for the alluvial fans in Coprates Chasma and Juventae Chasma in Valles Marineris (Table S1). Also shown are HiRISE (Figure S2, S5) and CRISM (Figure S4) observations of Coprates Chasma fans. Figure S3 shows the fan apices and catchment areas for Coprates and Juventae Chasma fans. Figure S6 shows the topographic setting of the Juventae Chasma fans. CTX and HiRISE observations of the Juventae Chasma fans are shown in Figure S7. Figure S8 shows a conceptional model of the evolution of the Coprates Chasma canyon. Finally, Table S2 provides the image identification numbers used in all figures.

Production of stereo southeast Coprates Chasma CTX DEM mosaic

Digital elevation models (DEMs) were produced from CTX stereo images using the USGS Integrated Software for Imagers and Spectrometers (ISIS) software and the BAE photogrammetric package SOCET SET according to the method of Kirk et al. (2008). We selected 10 CTX image pairs to maximise coverage of the canyon. Tie points were automatically populated in SOCET SET between each image pair. We ran a series of bundle adjustments, removing erroneous tie points until the remaining points had an RMS pixel matching error of ≤ 0.6 pixels. The resultant DEM was then tied to Mars Orbiter Laser Altimeter (MOLA; Zuber et al., 1992) topography and exported with a horizontal post spacing of 20 m/pixel. We then exported orthorectified images from SOCET SET at a resolution of 6 m/pixel. The orthorectified images and DEMs were then mosaicked in ArcGIS. Finally, the orthorectified image mosaic was blended in Adobe Photoshop to remove seamlines using the Avenza Geographic Imager extension, which retains geospatial information in the blended product. We also produced an additional CTX DEM of alluvial fans in Juventae Chasma, where coverage was available.

Data availability

The standard remote sensing data products used here are available from the NASA Planetary Data System (https://pds.jpl.nasa.gov/). The CTX ortho images and digital elevation models are availabe for download from Figshare (https://doi.org/10.6084/m9.figshare.c.5306507.v1).

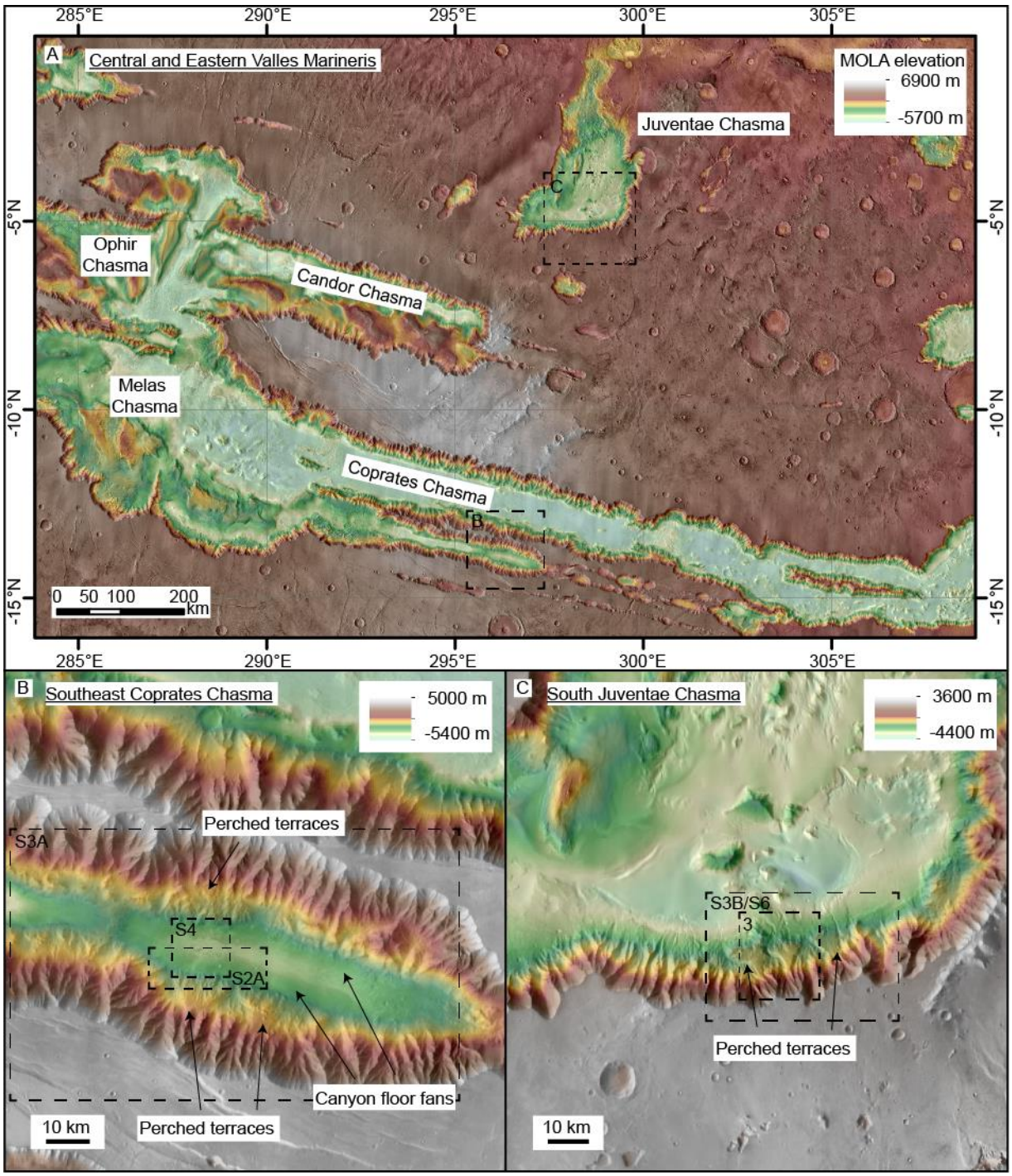

Figure S1: (A) Mars Orbiter Laser Altimeter (MOLA; Zuber et al., 1992) topographic map overlaid on THEMIS-IR day basmap showing the central and eastern Valles Marineris canyons. (B) MOLA topographic map overlaid on THEMIS-IR day basmap showing part of southeast Coprates Chasma, where the perched terraces and canyon floor fans are found. (C) MOLA topographic map overlaid on THEMIS-IR day basmap showing the southern wall of Juventae Chasma where the perched terraces are found.

Study site	Gen.	Fan	Lat/Lon of apex†	Apex elevation	Fan catchment (km^2)	Fan area (km^2)	Fan slope (degrees)	Cathment relief (km)
SE Copr.*	C1	C1_A	-13.95°, 295.55°	-74.88	-	8.20	9.31	-
SE Copr.	C1	C1_B	-14.12°, 296.18°	-422	-	5.18	8.47	-
SE Copr.	C1	C1_C	-14.15°, 296.12°	-273.45	-	7.01	10.71	-
SE Copr.	C1	C1_D	-14.23°, 296.38°	-124.1	-	7.70	8.82	-
SE Copr.	C1	C1_E	-14.24°, 296.33°	-154.46	-	7.72	7.33	-
SE Copr.	C1	C1_F	-13.63°, 296.18°	-467.93	-	3.55	6.45	-
SE Copr.	C2	C2_A	-13.75°, 295.98°	-2510.46	65.41	24.25	5.78	6.57
SE Copr.	C2	C2_B	-13.98°, 296.13°	-2668.10	290.91	9.65	11.34	5.07
SE Copr.	C2	C2_C	-14.03°, 296.27°	-2386.05	146.20	68.38	7.59	6.76
SE Copr.	C2	C2_D	-14.1°, 296.48°	-2285.82	215.82	31.07	9	6.72
SE Copr.	C2	C2_E	-14.17°, 296.64°	-2063.17	0.00	40.31	8.81	6.65
SE Copr.	C2	C2_F	-13.9°, 296.62°	-2686.17	65.41	9.18	7.42	6.74
SE Copr.	C2	C2_G	-13.97°, 296°	-2443.68	315.86	34.11	7.68	6.85
SE Copr.	C2	C2_I	-13.85°, 296.5°	-2587.83	109.10	19.64	8.65	6.85
SE Copr.	C2	C2_J	-13.75°, 296.37°	-2334.81	210.70	62.72	7.78	7.19
SE Copr.	C3	C2_K	-13.78°, 295.53°	-2289.47	78.62	5.76	9.01	7.02
SE Copr.	C3	C2_L	-13.81°, 296.64°	-2289.48	78.53	5.88	7.73	6.67
SE Copr.	C2	C2_M	-13.77°, 296.1°	2658.55	179.96	4.73	8.31	7.2
SE Copr.	C2	C2_N	-13.91°, 296.68°	-2567.51	315.86	8.23	7.36	6.91
SE Copr.	C2	C2_O	-14.12°, 296.55°	-2355.47	109.10	28.88	8.01	6.67
SE Copr.	C2	C2_P	-13.78°, 296.24°	2638.11	210.70	6.09	8.82	7
SE Copr.	C2	C2_Q	-13.85°, 296.78°	-2243.34	137.53	12.04	6.74	6.77
SE Copr.	C2	C2_R	-13.89°, 296.56°	-2791.45	-	5.66	8.81	-
SE Copr.	C3	C3_A	-13.98°, 296.13°	-2550.64	-	0.76	7.32	-
SE Copr.	C3	C3_B	-13.98°, 296.18°	-2681.36	-	0.54	8.83	-
SE Copr.	C3	C3_C	-14.01°, 296.28°	-2685.19	-	1.05	4.67	-
SE Copr.	C3	C3_D	-13.98°, 296.12°	-2625.75	-	0.80	10.9	-
SE Copr.	C3	C3_E	-13.99°, 296.16°	-2467.27	-	0.62	10.51	-
SE Copr.	C3	C3_F	-14°, 296.22°	2714.74	-	0.97		
Juventae	J1	J1_A	-5.16°, 298.68°	-747.47	-	18.61	6.29	-
Juventae	J1	J1_B	-5.2°, 298.56°	-468.44	-	19.68	6.8	-
Juventae	J1	J1_C	-5.1°, 298.87°	-1076.32	-	30.54	6.06	-
Juventae	J2	J2_A	-5.01°, 298.75°	-2341.29	211.08	76.63	4.84	5.18
Juventae	J2	J2_B	-5.02°, 298.61°	-2512.62	118.98	23.91	4.77	5.15

*SE Copr. = Southeast Coprates. σ = Extracted from MOLA.

† = Where apex is not clear, most upslope location is given

Table S1: Morphometrics of alluvial fans in SE Coprates and Juventae Chasma. Fan naming convention: e.g., C1 = The first generation (oldest) of Coprates fans; J2 = The second generation (youngest) of Juventae fans. Numbers have been assigned with decreasing age: e.g., C1 is older than C2, which is older than C3. Each individual fan within a generation has also been assigned a letter: e.g., C2_E = Fan E within the second generation of Coprates fans. Catchment area and fan surface slope measurements were made using available CTX DEMs and the ArcGIS hydrology toolkit. Catchment measurement were only made where the catchment was well-preserved and clearly linked to the fan apex. This was only possible for the C2 and J2 generations of fans. For

the C1 and J1 fans, the catchment has been overprinted. For the C3 fans, their small size meant their apices could not be fitted to the flow direction raster and attempts to reconstruct a hydrological catchment were unsuccessful.

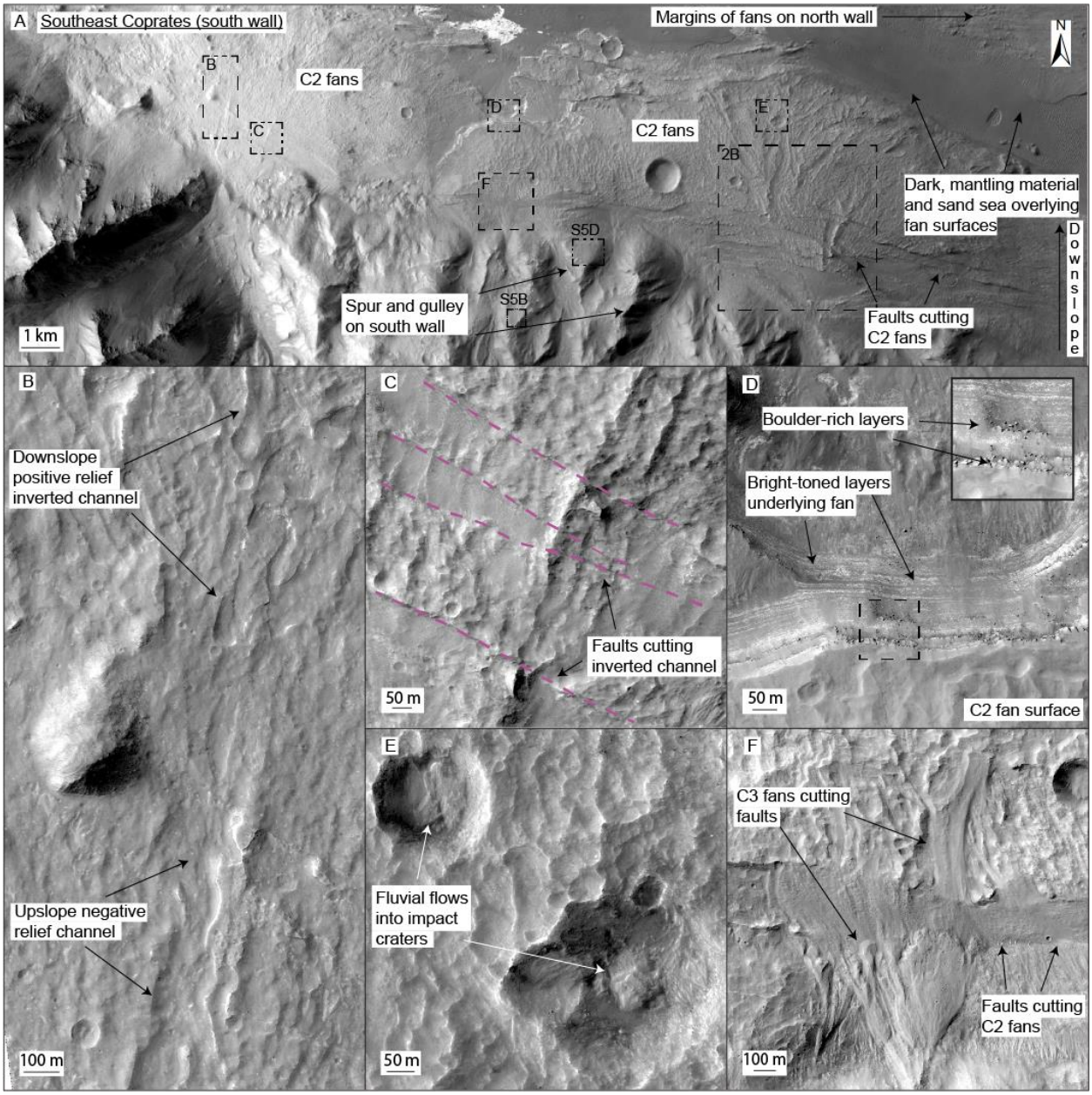

Figure S2: (A) CTX image mosaic of alluvial fan deposits and bajadas on southern wall of Southeast Coprates Chasma canyon. (B) HiRISE images of negative relief on C2 fan surface transitioning downslope into (positive relief) inverted channel, likely due to increased erosion. (C) HiRISE image of inverted channel on C2 fan surface which has been cut by multiple faults. (D) HiRISE image into backwasted margins of C2 alluvial fans, exposing sub-horizontal layering. Darker, boulder-rich layers overlie, bright-toned layers which may be associated with possible playas. (E) HiRISE image of embedded impact craters on C2 fan surfaces. These impact

craters has formed in between episodes of sedimentation and have sequentially been infilled by later fluvial deposits. Their presence points to hiatuses between flow events. (F) HiRISE image of C3 alluvial fans, which cut across the faulted C2 fan surfaces.

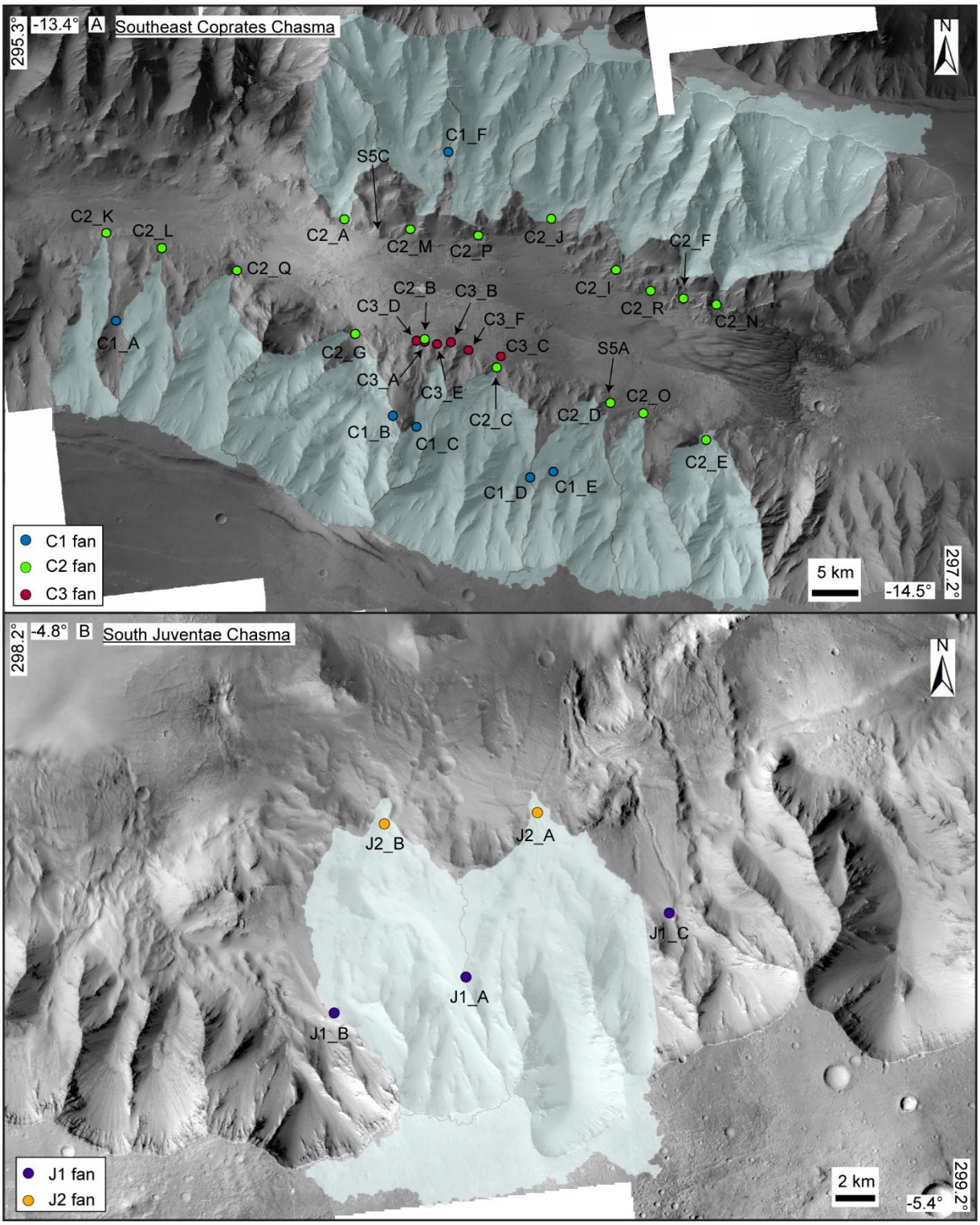

Figure S3: (A) CTX mosaic showing SE Coprates Chasma. The coloured circles show the apices for three generations of sediment fans (C1, C2, C3). The shaded blue area shows the reconstructed catchment for the C2 fans. (A) CTX mosaic showing south Juventae Chasma. The coloured circles show the apices for two generations of sediment fans (J1, J2). The shaded blue area shows the reconstructed catchment for the J2 fans.

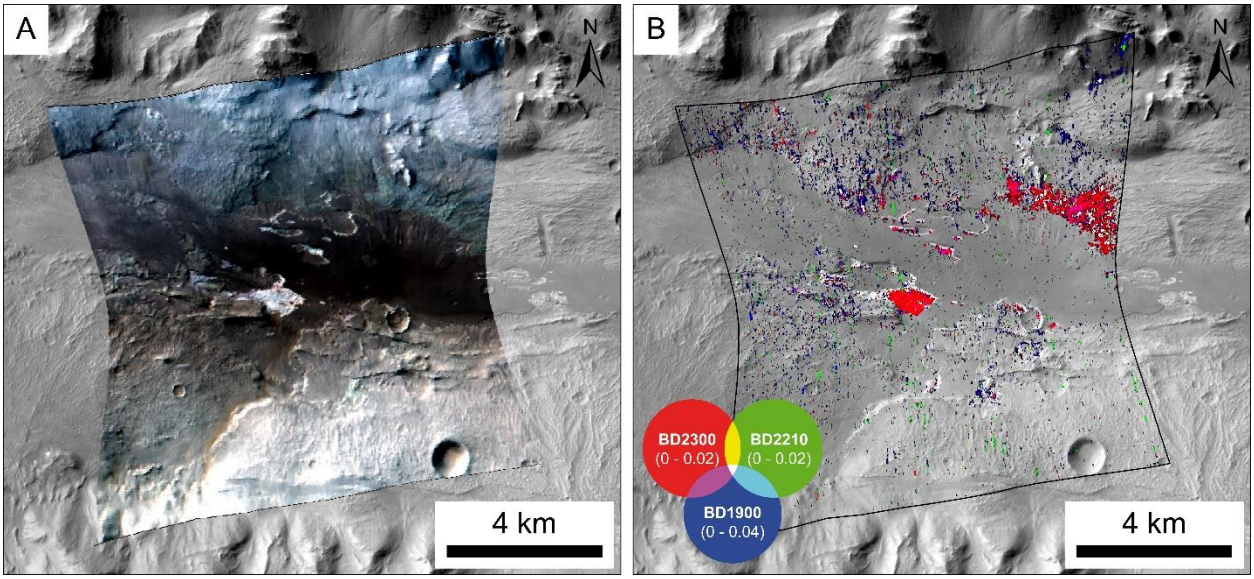

Figure S4: Likely presence of hydrous minerals in sedimentary material in SE Coprates Chasma. (A) CRISM false-colour image of canyon floor. Image FRT0000ABB7, processed using standard techniques (e.g. Murchie et al., 2007; 2009). (B) CRISM phyllosilicate spectral parameter map of the light-toned layered deposits in the center of the southeast Coprates Chasma basin. Spectral parameters derived using standard techniques (e.g. Viviano-Beck et al., 2014)). Red = BD2300, green = BD2210, blue = BD1900. Hydroxylated and hydrated silicates, probably mostly Fe/Mg-rich (identified from 2.3 micron absorption feature), are confined to outcrops of light-toned material, or where darker material appears thinner, occurring at the lowest elevations and the distal end of depositional fan material. BD = band depth. Detections are similar to those which occur in the adjacent SE Coprates Catena to the east (Grindrod et al., 2012; 2018).

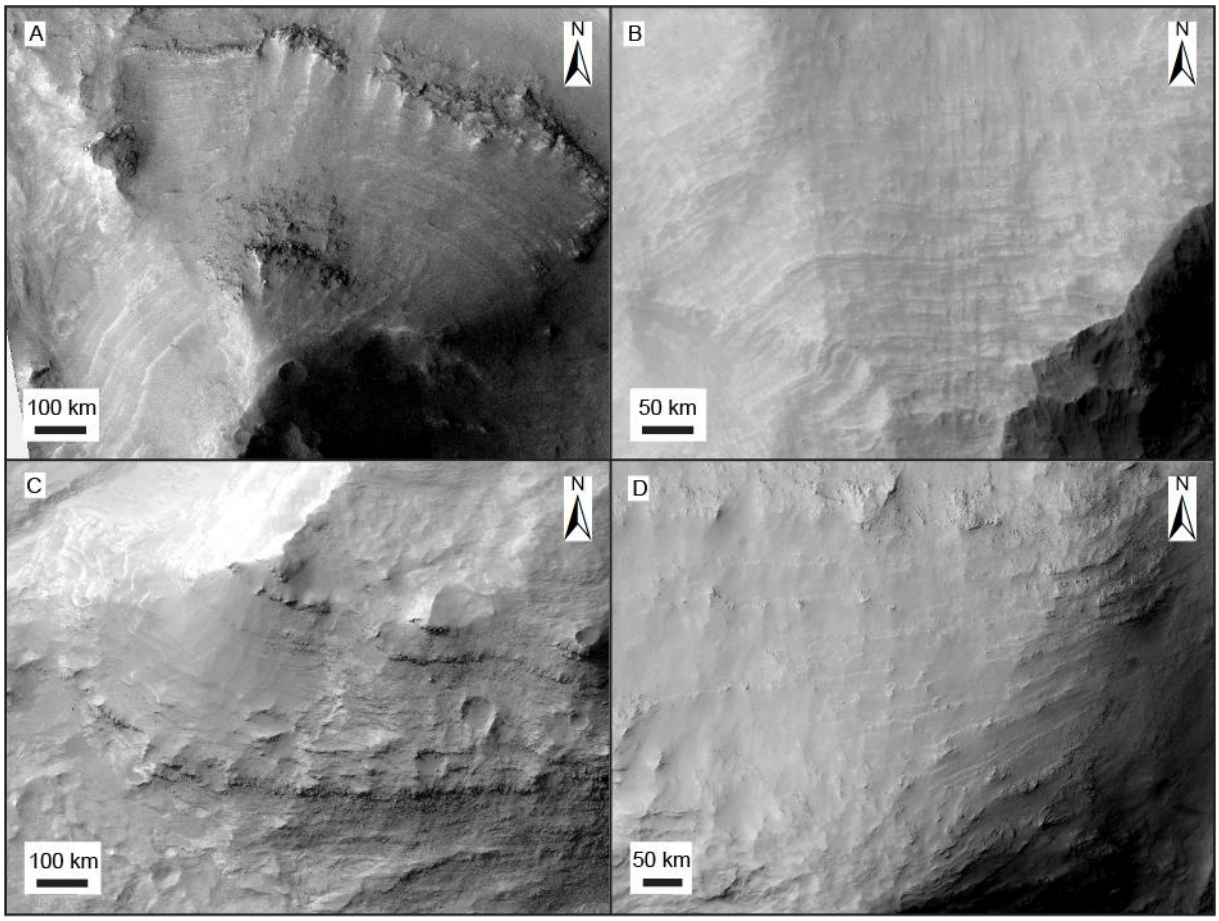

Figure S5: Examples of layered deposits visible in HiRISE images found in both the north and south wall of the SE Coprates Chasma study site. The layered deposits are found in the canyon wall between the C1 and C2 fan deposits (see Fig. 1). We interpret these layered deposits as sedimentary deposits, likely a combination degraded remnants of C1 sediment fans and the underlying sediment basement material. We note that the layered deposits are only visible in HiRISE images. There is currently no HiRISE coverage above the elevation of the C1 fans and CTX images suggests that the layered deposits do not occur here. See Fig. S2 and S3 for context locations.

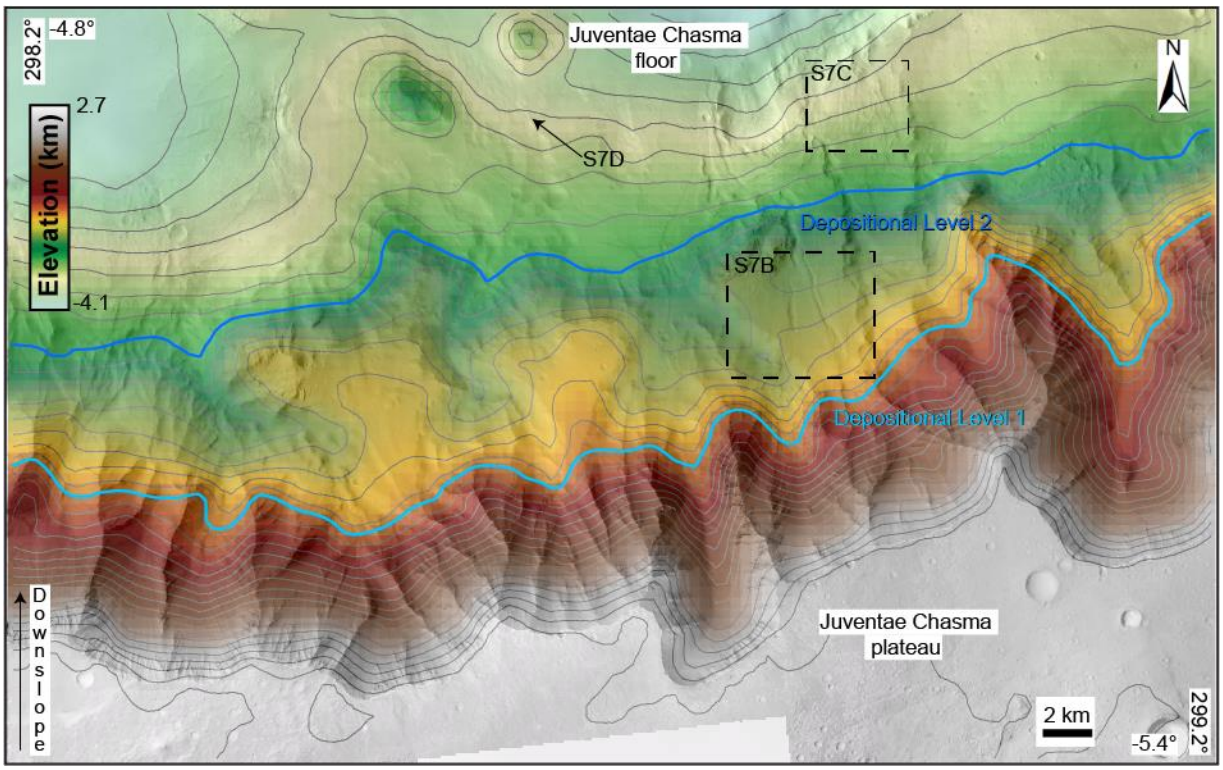

Figure S6: Stereo MOLA topographic map of Juventae Chasma study site, overlaid on CTX basemap mosaic showing vertically separated levels of sediment deposition clustered at ~ -850 m and ~ -2400 m.

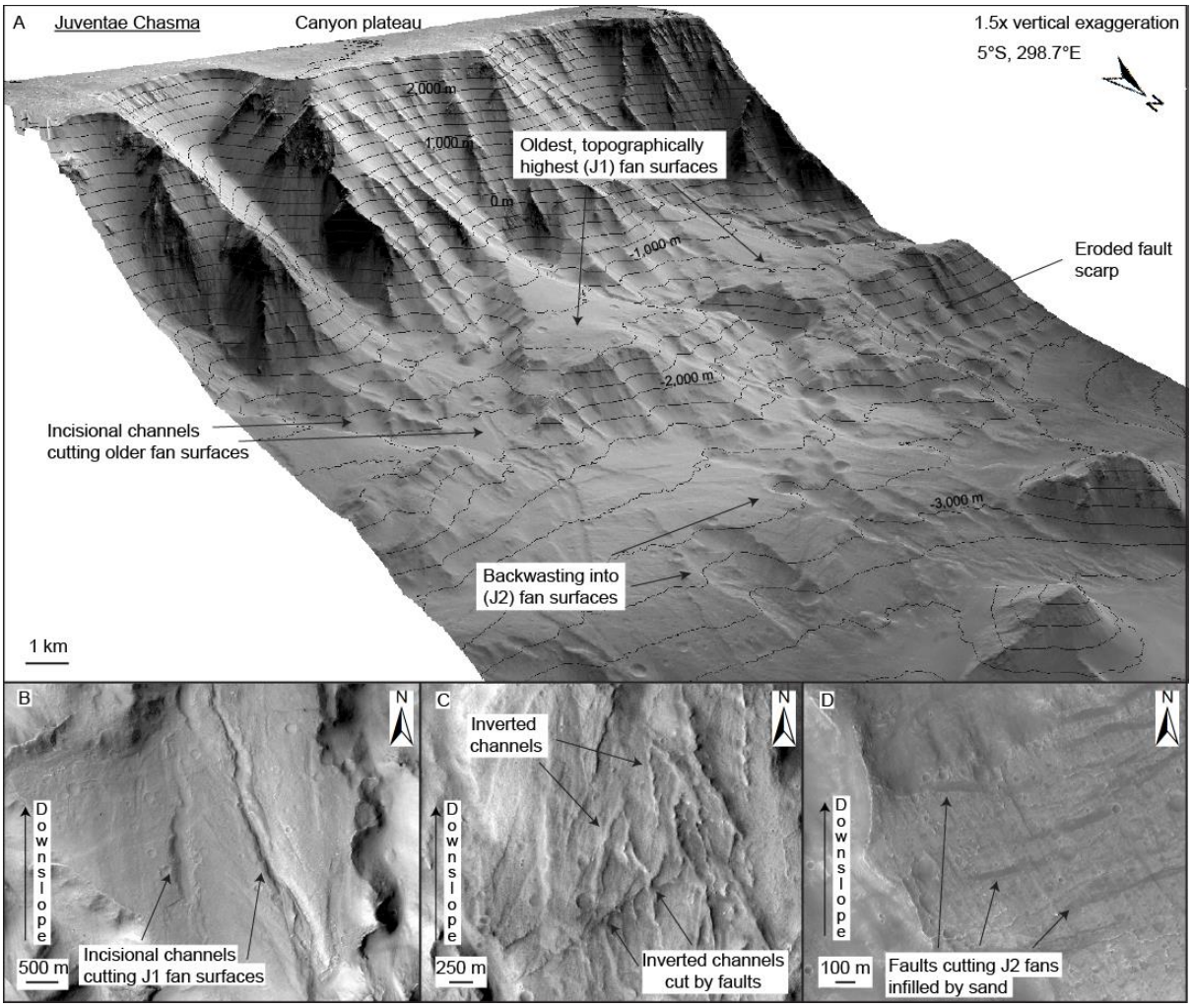

Figure S7: (A) Oblique CTX view of perched terraces, interpreted as faulted alluvial fan deposits, on the southern wall of Juventae Chasma. At least two generations (J1 & J2) of alluvial fan deposits are visible, which are found at similar elevations along the canyon wall. Some remnant channels are visible on their surfaces. Like in Coprates Chasma, the oldest (J1) fan surfaces are over a kilometer from the canyon floor. The J2 fans have also been left relatively uplifted. A third generation of alluvial fan deposits may exist on the current canyon floor, although these are buried by an extensive sand sea. Contours are shown at 200 m intervals. The morphometrics of these fans are shown in Table S1. (B) CTX image showing incisional channels that cut through the J2 fans. (C) CTX showing faulted inverted channels on J2 fan surfaces. (D) HiRISE image showing faults on J2 fan surface which have become infilled with sand.

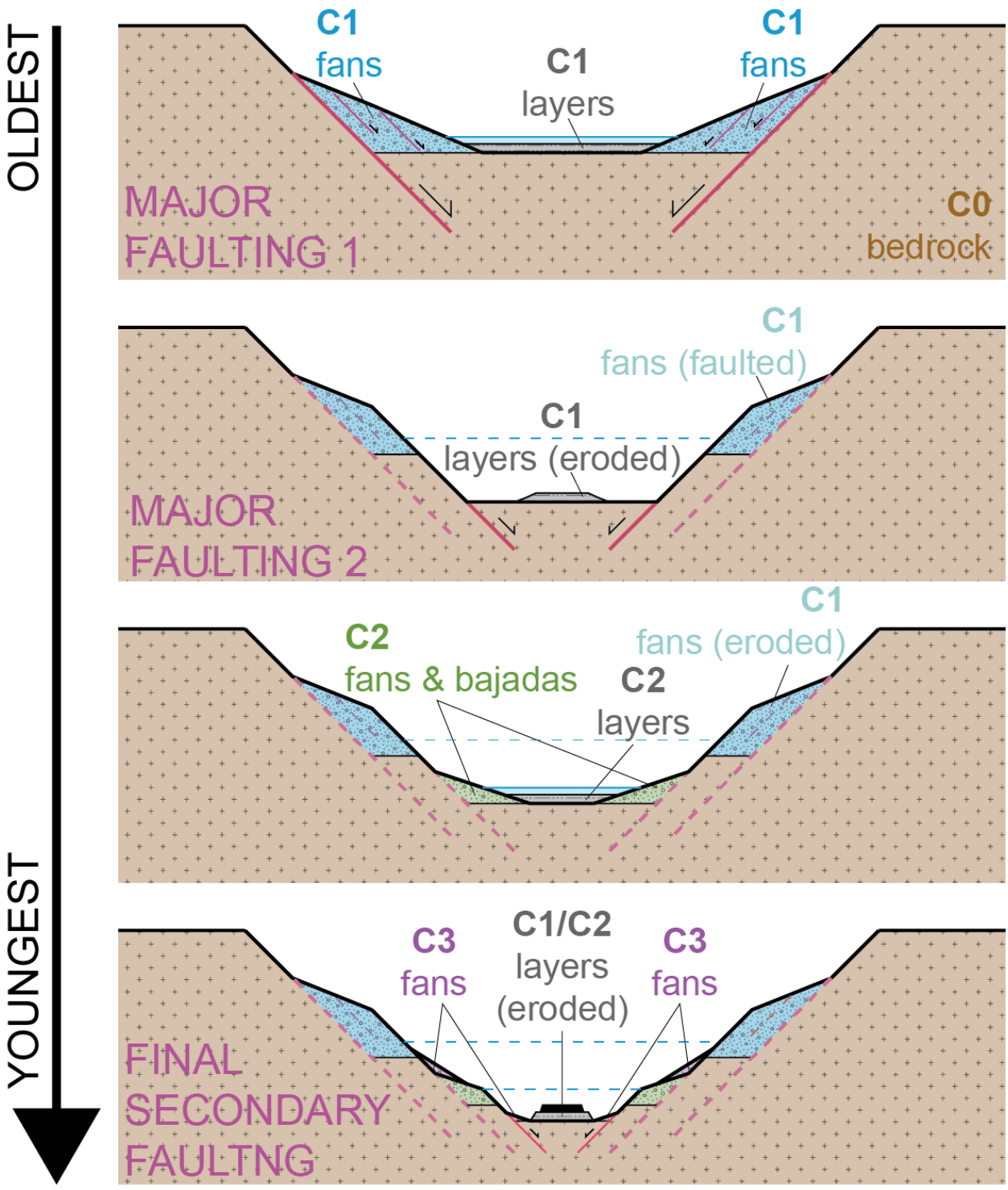

Figure S8: Simplified conceptual model showing multi-stage evolution of southeast Coprates Chasma. Successive generations of alluvial fans have formed as the canyon developed, assuming a progressive, basinward shift in normal faulting. Associated synthetic faults have cut the fan surfaces. Not to scale.

Figure	Instrument	Image ID
1	CTX (DEM)	D21_035265_1668_XN_13S063W
		D21_035542_1668_XN_13S063W
		D18_034118_1660_XN_14S064W
		D21_035476_1672_XN_12S064W
		G04_019824_1673_XN_12S065W
		P07_003711_1680_XN_12S065W
		P08_004067_1681_XN_11S064W
		P12_005913_1642_XI_15S063W
		D19_034619_1672_XN_12S064W
		P06_003355_1673_XI_12S064W
		J01_045340_1658_XN_14S063W
		J11_048966_1660_XN_14S063W
		B02_010475_1667_XI_13S063W
		J01_045129_1667_XI_13S063W
		F02_036597_1674_XN_12S065W
		P14_006546_1670_XN_13S065W
		J05_046619_1666_XN_13S062W
		J09_048254_1668_XN_13S063W
2a	CTX (DEM)	B02_010475_1667_XI_13S063W
		J01_045129_1667_XI_13S063W
2b	HiRISE	ESP_060465_1660
		ESP_060465_1660
2c	CTX	B02_010475_1667_XI_13S063W
		J01_045129_1667_XI_13S063W
3	CTX	D10_030940_1752_XN_04S061W
		D09_030795_1752_XN_04S061W
S1A	MOLA, THEMIS-IR Day	Global mosaic
S1B	MOLA, THEMIS-IR Day	Global mosaic
S1C	MOLA, THEMIS-IR Day	Global mosaic
S2A	CTX	J01_045129_1667_XI_13S063W
		P12_005913_1642_XI_15S063W
S2B	HiRISE	ESP_061098_1660
S2C	HiRISE	ESP_061098_1660
S2D	HiRISE	PSP_008339_1660
S2E	HiRISE	ESP_060043_1660
S2F	HiRISE	PSP_008339_1660
S3A	CTX	Same as Fig. 1
S3B	CTX	D10_030940_1752_XN_04S061W
		J04_046342_1770_XN_03S061W
		P15_007060_1770_XN_03S062W
S4	CRISM	FRT0000ABB7
	CTX	P12_005913_1642_XI_15S063W
S5A	HiRISE	ESP_061098_1660
S5B	HiRISE	PSP_008339_1660
S5C	HiRISE	PSP_008339_1660
S5D	HiRISE	ESP_055625_1660
S6	MOLA	Global mosaic
	CTX	D10_030940_1752_XN_04S061W
		J04_046342_1770_XN_03S061W
		P15_007060_1770_XN_03S062W
S7A	CTX (DEM)	D10_030940_1752_XN_04S061W
		D09_030795_1752_XN_04S061W
S7B	CTX	D10_030940_1752_XN_04S061W

S7C	CTX	B20_017424_1773_XN_02S061W
S7D	HiRISE	PSP_006203_1750

Table S2: List of instruments and image IDs used in figures.

References

Grindrod, P.M., Warner, N.H., Hobley, D.E.J., Schwartz, C., and Gupta, S., 2018, Stepped fans and facies-equivalent phyllosilicates in Coprates Catena, Mars: Icarus, v. 307, p. 260–280, doi:10.1016/j.icarus.2017.10.030.

Grindrod, P.M., West, M., Warner, N.H., and Gupta, S., 2012, Formation of an Hesperian-aged sedimentary basin containing phyllosilicates in Coprates Catena, Mars: Icarus, v. 218, p. 178–195, doi:10.1016/j.icarus.2011.11.027.

Kirk, R.L., Howington-Kraus, E., Rosiek, M.R., Anderson, J.A., Archinal, B.A., Becker, K.J., et al. (2008). Ultrahigh resolution topographic mapping of Mars with MRO HiRISE stereo images: Meter-scale slopes of candidate Phoenix landing sites. Journal of Geophysical Research, 113, E00A24, https://doi.org/10.1029/2007JE003000.

Murchie, S., et al. (2007), Compact Reconnaissance Imaging Spectrometer for Mars (CRISM) on Mars Reconnaissance Orbiter (MRO), Journal of Geophysical Research, 112, E05S03, https://doi.org/10.1029/2006JE002682.

Murchie, S., et al. (2009), Evidence for the origin of layered deposits in Candor Chasma, Mars, from mineral composition and hydrologic modeling, Journal of Geophysical Research, 114, E00D05, https://doi.org/10.1029/2009JE003343.

Viviano- Beck, C. E., et al. (2014), Revised CRISM spectral parameters and summary products based on the currently detected mineral diversity on Mars, J. Geophys. Res. Planets, 119, 1403– 1431, doi:10.1002/2014JE004627.

Zuber, M.T., Smith, D.E., Solomon, S.C., Muhleman, D.O., Head, J.W., Garvin, J.B., et al. (1992). The Mars Observer laser altimeter investigation. Journal of Geophysical Research, 97, 7781–7797. https://doi.org/10.1029/92JE00341